A Thin-ply Composite with Embedded Metallic Mesh for a Spaceborne Antenna

Jonathan Mihaly
Jet Propulsion Laboratory,
California Institute of Technology
4800 Oak Grove Dr.
Pasadena, CA 91109
Jonathan.M.Mihaly@jpl.nasa.gov

Maria Sakovsky
California Institute of Technology
1200 E. California Blvd.
Pasadena, CA 91125
msakovsk@alumni.caltech.edu

***Abstract* — Composite materials are well established in the space industry and offer significant strength-to-weight advantages for large-scale structures. However, composite materials with embedded conductive elements have not been implemented in spaceborne antenna systems as radiating elements. Furthermore, the use of composite materials for deep space missions requires the materials to be robust to extreme temperatures. Microcracking and delamination between fiber and matrix components, as well as the conductive element, presents an inherent limitation in the application of composite materials to cryogenic temperatures. Thin-ply laminates (ply thickness of less than 70 μm) have been identified as a technique to mitigate microcracking, however little data exists in open literature that aids the design and fabrication of such structures. This study presents a technique developed for embedding a conductive metallic mesh into the layup of thin-ply carbon fiber reinforced polymer (CFRP) composite material. Thermal cycling and subsequent mechanical testing on fabricated samples has been used to evaluate thin-ply composites as a crack mitigation technique. Furthermore, the construction of thin-ply CFRP composite tubes has been demonstrated for both straight segments and curved segments utilizing a novel sacrificial ceramic molding method. These prototypes represent the building blocks for a 1 m scale radiating element and are the first test articles for the evaluation of thin-ply CFRP composites with an embedded metallic mesh. The successful implementation of a CFRP composite with an embedded metallic mesh would enable ultra-lightweight conductive structures for future applications, such as antennas, requiring survival in cryogenic temperatures.**

TABLE OF CONTENTS

1. INTRODUCTION

Fiber composite materials are used in a variety of applications for space structures. Compared to conventional aerospace metals, composite materials provide a significantly higher Young's modulus (stiffness) relative to material density, but have anisotropic conductivity, requiring additional design considerations to be utilized as antenna radiating elements [1, 2]. Embedding metallic mesh into composites presents one potential method of maintaining structural benefits while adding the electrical conductivity required for utility as an antenna radiating element. Antennas constructed using this technique have predictable electromagnetic performance [3]. However, composites with embedded metallic meshes have never been qualified or used as radiating elements for spaceborne applications.

The use of composite materials for space missions requires the materials to be robust to severe temperatures ranges. Microcracking and delamination between fiber and matrix components present an inherent limitation in the application of composite materials to cryogenic temperatures as repeated thermal cycling could lead to degraded mechanical properties and structural failure [4, 5]. The use of thin-ply laminates (ply thickness of less than 70 μm) in the fabrication of composite layups have been identified as a technique to mitigate microcracking both at room temperature and in cryogenic testing [6-8], as experimental studies have demonstrated the ability of thin-ply composites to suppress and delay the onset of microcracking. The observed trends are hypothesized to be due to smaller cracks as a result of high crack propagation energy at the ply boundaries as well as statistically less defects in thin-ply composites [7]. This approach is advantageous over other methods of mitigating microcracks, as thin-ply composites at the same time increase material performance resulting in higher stiffness, improved strength, and better damage resistance [6, 7].

Therefore, the developed approach to utilizing a composite material for a spaceborne antenna element involves the fabrication of a carbon fiber composite layup consisting of thin-ply composites cured with an embedded metallic mesh. This represents a novel approach to simultaneously addressing the thermal and electrical limitation of conventional composite materials.

2. MATERIALS

The proposed electrically conductive composite material consists of two primary components: thin-ply (~30 μm/ply) carbon fiber reinforced polymer (CFRP) and a metallic mesh. The CFRP consists of unidirectional M55JB-6K carbon fiber with a Thinpreg120 epoxy resin reinforcement obtained as a prepreg tape from North Thin Ply Technology [9]. The fiber was selected for its high modulus, ideal for thin-ply applications, whereas the resin was selected for its high glass transition temperature of 180°C, appropriate for the large range of operating temperatures found in space.

The woven phosphor bronze mesh from TWP Inc. [10] is a twill weave composed of wires with a diameter of 114 microns, easily satisfying the typical five times of the skin-depth requirement for 30 to 1000 MHz. The mesh opening is 140 microns ($\ll \frac{\lambda}{100}$ for VHF and UHF) and has no significant impact on the electromagnetic performance.

The antenna radiating element considered herein is envisioned as a thin-walled circular cross-section. Figure 1 provides two options considered for the composite cross section, one with the metallic conductor on the exterior (a) and alternatively with the metallic layer several plies into the layup (b). Regarding the thickness of each component, t_{CF} and t_c denote the thickness of the CFRP and metallic mesh, respectively. For a 1 mm thick cross-section, the corresponding areal density is 1.74 kg/m^2 (including the metallic mesh). For comparison, an aluminum antenna with the same cross-section would have a density of 2.70 kg/m^2.

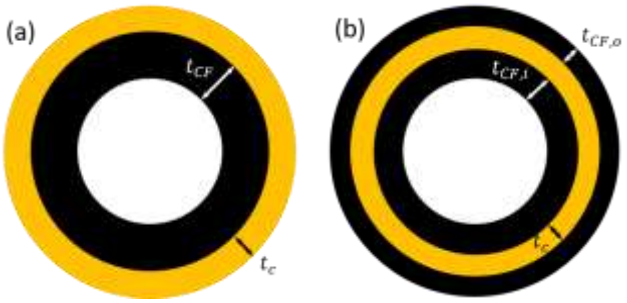

FIGURE 1: *Proposed composite antenna cross-sectional geometry. Carbon fiber and metallic mesh indicated in black and yellow, respectively. (a) Metallic mesh embedded on exterior. (b) Metallic mesh embedded inside carbon fiber layup.*

3. VALIDATION OF THIN-PLY APPROACH

The proposed design approach of using thin-ply composites to mitigate microcracking was validated by thermal cycling flat coupon samples (1 × 10 in.^{2}) with varying ply thickness and monitoring crack formation and stiffness. All samples were manufactured using the previously described prepreg material (in Section 2) with the effective ply thickness increased by stacking multiple plies with the same fiber direction. The same prepreg material is used for all samples to minimize the effects of the prepreg fabrication process on the results. Five coupons of each of the samples described in Table 1 were fabricated and tested. The samples tested three ply thicknesses (samples A, B, and C) as well as the effects of embedding conductive mesh on the outer ply and inside the composite layup (samples AO and AI).

Sample ID	Layup	Mesh Location	Effective Ply Thickness (μm)
A	$[0\backslash\pm45\backslash90\backslash\mp45\backslash0]_3$	None	30
B	$[\mp45_2\backslash0_2\backslash\pm45_2\backslash90]_s$	None	60
C	$[0_3\backslash\pm45_3\backslash90_3\backslash\mp45_3\backslash0_3]$	None	90
AO	$[0\backslash\pm45\backslash90\backslash\mp45\backslash0]_3$	Outer ply	30
AI	$[0\backslash\pm45\backslash90\backslash\mp45\backslash0]_3$	Inside layup	30

TABLE 1: *Samples used in thermal testing*

All samples were first subjected to five low-level thermal cycles from -55°C to 180°C in an INSTRON 3119-506 thermal chamber, to evaluate the effects of ply thickness on the extent of microcracking. Following this were five thermal shock cycles achieved by dipping samples into liquid nitrogen (-196°C) followed by a bake out at 140°C. This allowed further insight into the microcracking behavior without the need for a large number of lengthy thermal cycles and is closer to the temperature range seen in a deep space mission. A 10 min dwell time was used at each temperature extreme.

The sample edges were polished prior to testing and examined for microcracking using a Nikon Eclipse LV150N optical microscope after each thermal cycle. Tension tests were conducted at 25°C before and after low-level thermal cycling and thermal shock testing following ASTM D3039M [11] to gauge the effects of microcracking on stiffness. The effects of microcracking on composite strength were not investigated here due to the destructive nature of the testing but should be investigated in future work.

Sections 3.1 – 3.3 describe the main experimental observations made relevant to the design of composite structures with embedded metallic meshes for a cryogenic environment.

3.1 EFFECT OF PLY THICKNESS ON MICROCRACKING

Figure 2 plots the microcrack density observed in the center 90° ply in samples A (30 μm plies), B (60 μm plies), and C

(90 μm plies) as a function of number of low-level thermal cycles. As predicted, the use of thin plies delays the onset of microcracking. The samples with the thinnest layers begin to exhibit a small number of cracks after five thermal cycles.

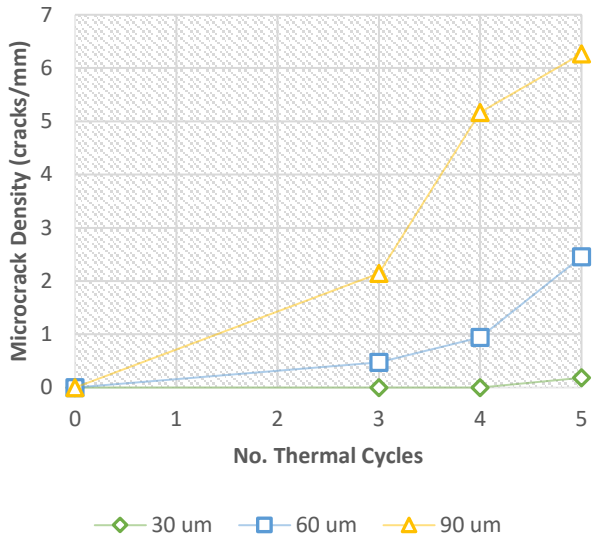

FIGURE 2: *Microcrack density as a function of number of thermal cycles for various ply thicknesses*

This trend occurs since the ply boundaries pose barriers to crack propagation, requiring a high crack propagation energy. Furthermore, it has been suggested that thin-ply composites contain less fabrication defects [7]. The latter was not evaluated in this study as not all samples could be cured at once resulting in slightly differing cure pressures with a potential impact on defect content.

Figure 3 (a) and (b) shows the characteristic of the cracks in the 90 μm and 30 μm samples, respectively, after 5 low-level thermal cycles. Thicker plies allowed cracks to branch and propagate parallel to the ply boundaries resulting in crack lengths of several mm in the 90 μm samples after 5 thermal cycles compared to only ~10 μm long cracks in the 30 μm samples.

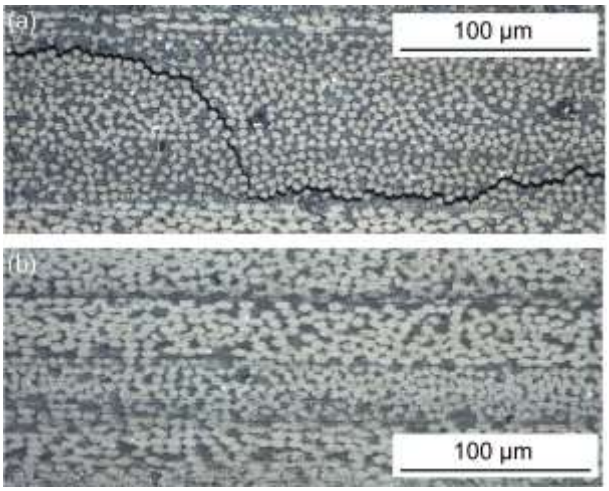

FIGURE 3: *(a) Cracks in 90 **μ**m plies, 50X magnification. (b) Cracks in 30 **μ**m plies, 50X magnification.*

After five low-level thermal cycles, no significant drop in stiffness at room temperature was measured in any of the samples, with moduli remaining within ±5% of those initially measured.

3.2 Contact Stresses Between Metallic Mesh and Fibers

It is worth noting that the coefficient of thermal expansion (CTE) mismatch between materials, which often drives and limits the survival temperature range for many composites, is actually smaller between the bronze mesh (~18 ppm/deg C) and carbon fiber (-1.1 ppm/deg C) than it is between the carbon fiber and the epoxy (45-55 ppm/deg C). However, the presence of the mesh still induces microcracking in the composite in several ways. First, due to contact stresses developed due to CTE mismatches. Second, due to bending induced by CTE mismatch of the metallic mesh layer and the composite.

At the cold end of the cycle, the epoxy matrix shrinks more than the metallic mesh embedded in it. As a result, the metallic wires (of radius R_c, with elastic constants E_c and ν_c) come in contact with the carbon fibers (of radius R_{CF}, with elastic constants E_{CF} and ν_{CF}) in the adjacent ply. A simplified Hertzian contact model between two perpendicular cylinders can be used to compute the approximate contact stresses. This case is equivalent to a sphere in contact with a plane where the maximum contact stress is given by [12],

$$\sigma_{max} = \sqrt[3]{\frac{1}{\pi}\frac{6FE_{eff}^2}{R_{eff}^2}}$$

where F is the maximum contact force given by,

$$F = \frac{4}{3}E_{eff}R_{eff}^{1/2}d^{3/2}$$

d is the contact depth resulting from the CTE mismatch between the epoxy and metallic mesh, $R_{eff} = (R_c^{-1} + R_{CF}^{-1})^{-1}$ is the effective sphere radius, and $E_{eff} = \left(\frac{1-\nu_{CF}^2}{E_{CF}} + \frac{1-\nu_c^2}{E_c}\right)^{-1}$ is the effective modulus.

Using the material properties given in references [13] and [10], the resulting contact stress from cooling the composite to -55ºC from a stress-free state at 25ºC is 0.95 GPa (low-level thermal cycling). The transverse compressive strength for the M55J fiber is not available in literature but it is expected to be only a small fraction of the strength in the fiber direction of 4 GPa due to anisotropy of carbon fiber. Hence, it is anticipated that the brittle carbon fibers will crack upon cooling.

This behavior was observed in all samples with embedded mesh (samples AO and AI) after five low-level thermal cycles. Figure 4 illustrates this effect in samples AI, where

transverse cracking of the carbon fibers can be seen below the middle conductive wire (in yellow). In fact, the breaks extend several fibers away from the conductive wire. Figure 4 is representative of observations in both samples AI and AO.

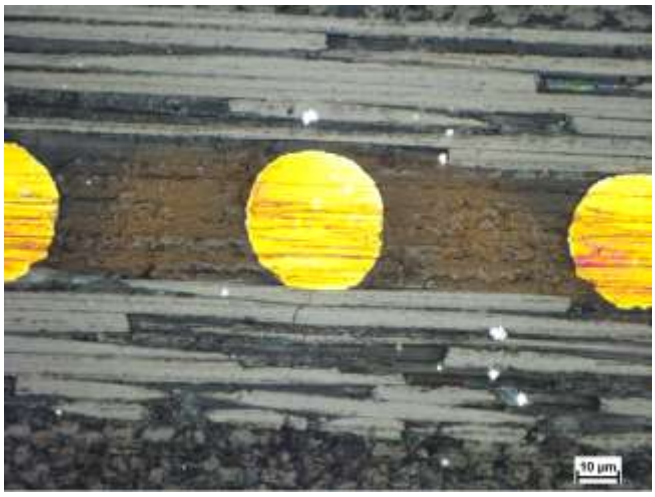

FIGURE 4: *Cracking of carbon fibers due to thermally induced contact stresses with metallic mesh in samples AI, 100X magnification.*

The observed cracking had no impact on the stiffness of the composite samples. Tension tests after 5 low-level thermal cycles measured moduli within ±5% of initial values.

3.3 Effect of Mesh Location

Due to the CTE mismatch of the conductive layer and the composite, the two will contract and expand by different amounts under thermal cycling. This results in a thermally induced curvature in the flat samples when the conductor is embedded on the outside of composite (i.e. samples AO). This effect is as described by Stoney in reference [14].

The temperature range in the initial low-level thermal cycling did not induce a sufficient curvature to crack the composite samples. However, Figure 5 shows a micrograph of sample AO after five thermal shock cycles. Severe microcracking was observed in these samples with cracks propagating though one ply after a single thermal shock cycle and though three plies after five shock cycles. All microcracking due to this effect was observed in the plies under compression.

In the samples with the conductive layer in the middle of the layup (i.e. samples AI), the conductor is constrained and cannot induce the same curvature. Hence, no microcracking was observed in samples AI after thermal shock testing.

The thermally induced curvature may be compensated for through geometry. For example, the effect may be unnoticeable for an isothermal circular CRFP tube with an outer conductor. However, this is an important consideration when designing arbitrary cross-sections with flat segments and even face sheets in sandwich panels.

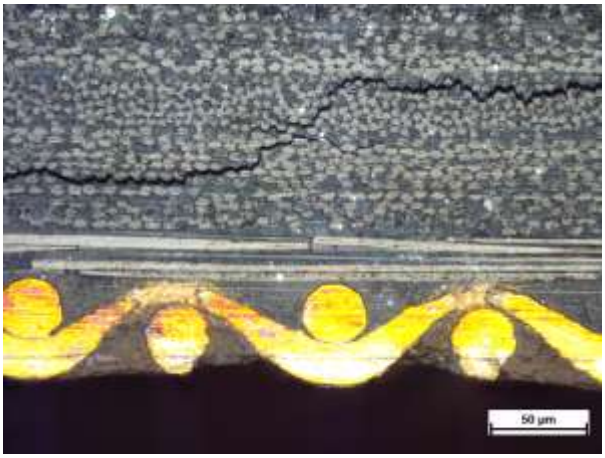

FIGURE 5: *Microcracking due to thermally induced bending in samples AO, 50X magnification.*

Tensile testing of samples AO after five thermal shock cycles revealed a drop in modulus between 18% and 25% in three out of five coupons (the other two coupons showed no significant change in modulus). This is in contrast to the effects of the microcracking observed after low-level thermal cycling where moduli remained within ±5% of initial values. The stress-strain curves for these three coupons before and after thermal shock testing are shown in Figure 6. Testing on a statistically significant sample size would be required to show that microcracking due to thermally induced bending can result in degraded material performance.

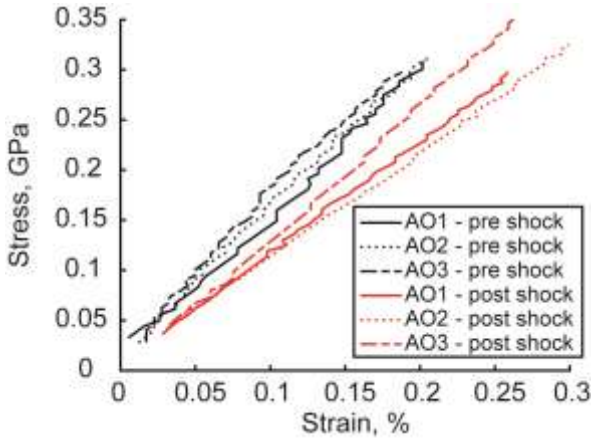

FIGURE 6: *Stress-strain curves for samples AO before (black) and after (red) thermal shock testing.*

The thermal testing presented in this section illustrated the ability of thin-ply composites to mitigate the formation of microcracks at cryogenic temperatures. The benefits were observed down to 30 µm ply thickness. Furthermore, the testing revealed two design considerations for embedding metallic meshes:

1) Contact stresses between the mesh and carbon fibers are sufficient to crack the carbon fibers. This does not degrade material modulus for the number of cycles tested.

2) The mesh should be embedded inside the composite layup to avoid thermally induced bending of the laminate, which may cause a large reduction in material modulus. The cross-sectional geometry can be used to compensate for this effect.

4. ANTENNA ELEMENT PROTOTYPES

Prototype antenna element segments were fabricated utilizing the materials and layup outlined in Section 2. A technique using a water-soluble sacrificial molding was developed to fabricate straight and curved tubes with the thin-walled circular cross section in Figure 1. Sacrificial molding allows for complex composite part geometries, in particular curved hollow sections where the composite tooling cannot otherwise be removed.

First, the water-soluble ceramic compound (Aquapour from Advanced Ceramics Manufacturing [15]) was cast into the required cylindrical shape using a 3D printed female mold. The ceramic starts as a powder, which is then mixed with water and degassed before being poured into the female mold. The 3D printed mold is composed of two pieces, with each piece covering 180° of the cylinder, so that it could easily be removed without damaging the ceramic. Figure 7 depicts the 3D printed female mold (a) used to cast the Aquapour ceramic mold (b). Utilizing a 3D printed mold enabled inexpensive and rapid prototype development, with each printed female mold capable of being reused.

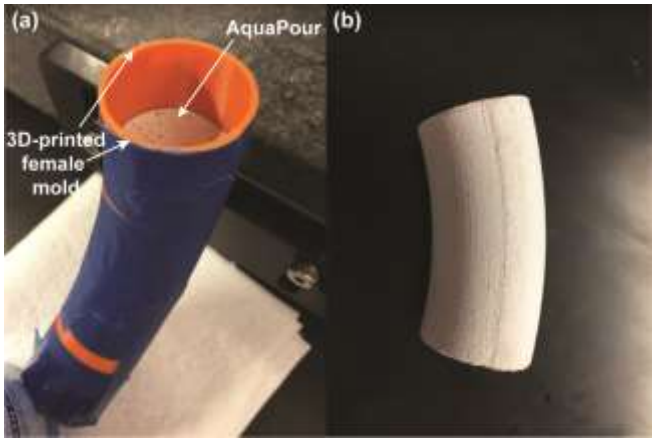

FIGURE 7: *(a) Two piece 3D-printed female mold for casting Aquapour ceramic mold. (b) Fully set ceramic mold.*

Once extracted from the 3D printed mold, the Aquapour ceramic mold is dehydrated in an oven at 110°C until 45% mass loss is achieved (~6 hours for a 35 mm diameter cylinder), sealed with the Aquaseal [15] compound to prevent epoxy infiltration during the cure, and then used for the lay-up of the composite material.

Special care was taken to layup the composite plies on the ceramic mold to prevent wrinkling of the prototypes. Wrinkles can form when thick layups are wrapped around a small radius due to the inability of plies to slip past one another. Therefore, as the plies were stacked, they were staggered by 50% of their width in the circumferential direction. Hence, as the layup was wrapped around the mold, at most two plies were wrapped at a time. In addition, heat-shrink tubing was applied on top of the composite layup to prevent wrinkles in the vacuum bagging from imprinting on the composite.

The composite material structure was cured at 120°C for 2 hours in an autoclave cure. Compared to metallic or plastic molds, the ceramic mold material has a smaller CTE mismatch with the carbon fiber composite material. This results in smaller residual stresses in the cured composite and allows for fabrication of more precise structures.

Finally, once the composite structure has cured, the ceramic mold is washed out using cold water. Figure 3(a) depicts a prototype composite tube segment with the ceramic mold partially dissolved away.

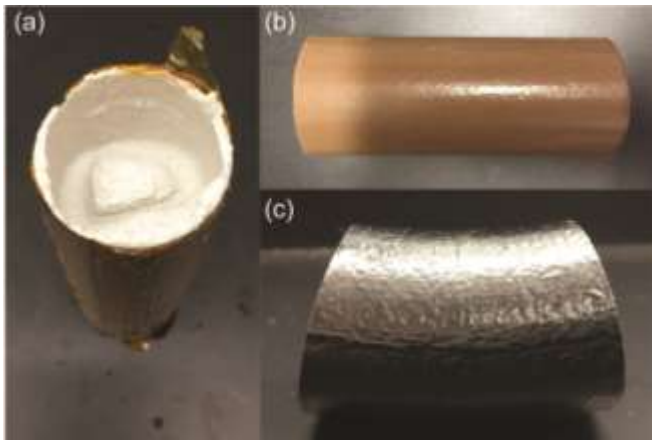

FIGURE 8: *(a) Prototype with ceramic mold partially washed away. (b) Straight tube prototype with embedded conductive mesh. (c) Curved tube prototype.*

Two types of prototype segments were manufactured with the described technique: straight hollow tubes with a diameter of 7 cm and a length of 20 cm (Figure 8(b)) and curved tube segments with a diameter of 7 cm, length of 10 cm, and a radius of curvature of the tube of 0.14 m (Figure 8(c)). The radius of curvature was selected for the future development of a full-scale UHF folded dipole utilizing this radius of curvature.

A quasi-isotropic $[\pm 45\backslash 0\backslash 90]_{s,n}$ composite layup was used for both segments, where s indicates that the layup is symmetric and n represents the number of times the layup is repeated ($n = 2$ was used for the straight tubes and $n = 1$ for the curved tubes). The straight tubes, furthermore had a conductive mesh embedded on the outside of the composite layup.

The fabricated prototypes serve as a proof-of-concept for the manufacture of large composite antenna elements with embedded metallic meshes. This technique can be scaled to build wire antenna topologies including the monopole, folded dipole, and Yagi arrays.

5. Conclusion and Future Work

A preliminary development and evaluation of a novel technique for the fabrication of isotropic electrically conductive composites for spaceborne application has been completed.

The composite layup described herein was shown to mitigate microcracking over low-level thermal cycles by utilizing thin ply laminates, consistent with previous studies [6-8]. While the addition of a metallic mesh did result in some cracking of carbon fibers local to the metal-carbon interface (as expected), such cracking was demonstrated to have no measurable effect on the stiffness of the material. Furthermore, no additional microcracking was observed following the thermal shock testing of the layup samples featuring the symmetric distribution of metallic mesh and CFRP laminates. Such results are promising for the future space qualification of metal-embedded thin-ply composites, which will require structural robustness over large temperature ranges. Future work will also include an extended thermal cycling test campaign with a larger sample size and temperature range for a more complete evaluation of the microcracking as a function of temperature extreme and cycling lifetime.

Additionally, the construction of thin-ply CFRP composite tubes – the building blocks of a radiating element – has been demonstrated for both straight segments (with embedded copper mesh) and curved segments (without embedded mesh). This fabrication technique will be extended in future work to complete a full-scale UHF folded dipole radiating element for RF field testing and performance comparison to conventional, metallic radiating elements.

The successful implementation of a CFRP composite with embedded metallic mesh would enable ultra-lightweight conductive structures for future applications, such as antennas, requiring survival in cryogenic temperatures. This advancement would be particularly beneficial for mass-critical missions and potentially enable previously implausible science instrumentation for small spacecraft and or deep space missions.

Acknowledgements

The research was carried out at the Jet Propulsion Laboratory, California Institute of Technology, under a contract with the National Aeronautics and Space Administration. The authors thank Professor Sergio Pellegrino for his support in providing materials and facilities for the prototyping effort leading to this work. The authors also thank Dr. Charles Elachi and Dr. Alina Moussessian for their guidance and support in facilitating this collaboration between JPL and Caltech.

References

Reference herein to any specific commercial product, process, or service by trade name, trademark, manufacturer, or otherwise, does not constitute or imply its endorsement by the United States Government or the Jet Propulsion Laboratory, California Institute of Technology.

[1] A. Mhdipour et al. “Reinforced Continuous Carbon-Fiber Composites Using Multi-Wall Carbon Nanotubes for Wideband Antenna Applications”, IEEE Transactions on Antennas and Propagation, 58(7), pg. 2451-2456, 2010.

[2] M. Lori et al. “Ultralight CFRP Horns”, 39th ESA Antenna Workshop, 2018.

[3] J. Costantine et al. “Deployable Helical Antennas for CubeSats”, IEEE Transactions on Antennas and Propagation, vol. 64(9), pg. 3752-3759, 2016.

[4] M. Sippel et al. “Progress on Advanced Cryo-Tanks Structural Design Achieved in CHATT-Project”, 14th European Conference on Spacecraft Structures Materials and Environmental Testing, 2016.

[5] D. Polis et al. “Cryogenic Durability of a Carbon Fiber Reinforced Cyanate Ester Composite: Degree-of-cure Effect”, International SAMPE Symposium and Exhibition, 2006.

[6] S. Sihn et al. “Experimental Studies of Thin-ply Laminated Composites”, Composites Science and Technology 67, 2007.

[7] R. Amacher et al. “Thin ply composites: experimental characterization and modeling of size-effects”, composites science and technology 101, pg. 121-132, 2014.

[8] K. Olofsson et al. “Thin-ply Micrometer Material Technology”, SICOMP Conference, 2016.

[9] North Thin Ply Technology, “Thin Ply Prepreg” url: www.thinplytechnology.com/products/thin-ply-prepreg, 2018.

[10] TWP Inc. “100 Mesh Bronze .0045”, url: https://www.twpinc.com/wire-mesh-material/bronze/100-mesh-bronze-0045, 2018.

[11] ASTM International. “ASTM D 3039M Standard Test Method for Tensile Properties of Polymer Matrix Composite Materials”, Annual Book of ASTM Standards, Volume 15.03, 2008.

[12] K. L. Johnson, “Contact mechanics”, Cambridge University Press, 1985.

[13] Toray Composite Materials American, Inc. “Types of Carbon Fiber”, url: www.toraycma.com/page.php?id=661, 2018.

[14] G. G. Stoney, “The Tension of Metallic Films Deposited by Electrolysis”, Proceedings of the Royal Society A, 83(553), pg. 172-175, 1909.

[15] Advanced Ceramics Manufacturing, “Aquapour”, url: www.acmtucson.com/acm_products/aquapour, 2018.

BIOGRAPHY

Jonathan Mihaly *received a Ph.D in Aeronautics from the California Institute of Technology in 2013. He has been with the Jet Propulsion Laboratory for 5 years. He is currently the Mechanical team lead for the REASON antennas on the Europa Clipper mission. Prior to joining REASON, he was an instrument systems engineer and lead flight engineer for the HyTES airborne instrument.*

Maria Sakovsky *received a Ph.D. in Space Engineering from the California Institute of Technology in 2018. She is currently a postdoctoral fellow at ETH Zurich. Her research interests lie in the application of composite materials to the space environment in particular for use in deployable and reconfigurable systems. She has worked with the JPL REASON team on the Europa Clipper mission to investigate the feasibility of an all-composite radar instrument.*